Research on the dynamic pressure effect of clearance oil film of stepped hydrostatic thrust bearing

Xiaodong Yu (yuxiaodong@hrbust.edu.cn)
Ministry of Education, Harbin University of Science and Technology

Yanan Feng
Ministry of Education, Harbin University of Science and Technology

Hui Jiang
Qiqihar Heavy CNC Equipment Corp. LTD

Weicheng Gao
Ministry of Education, Harbin University of Science and Technology

Guangqiang Shi
Ministry of Education, Harbin University of Science and Technology

Ruichun Dai
Qiqihar First Machine Tool Factory Corp. LTD

Wentao Jia
Qiqihar First Machine Tool Factory Corp. LTD

Junfeng Wang
Qiqihar First Machine Tool Factory Corp. LTD

Jianhua Jiao
Qiqihar Heavy CNC Equipment Corp. LTD

Research Article

Keywords: Step model, hydrostatic thrust bearing, clearance oil film, dynamic pressure effect

Posted Date: April 24th, 2023

DOI: https://doi.org/10.21203/rs.3.rs-2843402/v1

Additional Declarations: No competing interests reported.

Research on the dynamic pressure effect of clearance oil film of stepped hydrostatic thrust bearing

Xiaodong Yu[a], Yanan Feng[a], Hui Jiang[c], Weicheng Gao[a], Guangqiang Shi[a], Ruichun Dai[b], Wentao Jia[b], Junfeng Wang[b] and Jianhua Jiao[c]

(a. Key Laboratory of Advanced Manufacturing and Intelligent Technology, Ministry of Education, Harbin University of Science and Technology, Harbin 150080, China

b. Qiqihar First Machine Tool Factory Corp. LTD., Qiqihar 161005, China

c. Qiqihar Heavy CNC Equipment Corp. LTD., Qiqihar 161005, China)

Abstract: The dynamic pressure effect of the clearance oil film of stepped hydrostatic thrust bearing is studied by taking the double rectangular cavity oil cushion as an example. According to the hydrodynamics theory, the average dynamic pressure of lubricating oil film in different clearance height regions is theoretically deduced and calculated, and the dynamic pressure effect of the clearance oil film in the stepped hydrostatic thrust bearing is studied through the combination of theoretical calculation, simulation, and experimental verification. It is found that the theoretical value of the average dynamic pressure of the clearance oil film and the rotational speed show a linear growth relationship with a slope of 275.2. The simulated value of the average dynamic pressure and the rotational speed follow the growth law of the Fourier 1 model. The experimental value of the average dynamic pressure is between the theoretical value and the simulated value, which is basically not affected by the load. In the speed range of 0r/min-200r/min, compared with the viscosity of lubricating oil, the speed is the main factor affecting the dynamic pressure of the oil film of the stepped hydrostatic thrust bearing. The dynamic pressure value of the clearance oil film increases in a stepped fashion along the radial direction of the double rectangular cavity oil cushion. The dynamic pressure value has an obvious upward trend at the junction of the circumferential right oil cavity and the sealing edge and then decreases to 0 after reaching the peak value.

Keywords: Step model; hydrostatic thrust bearing; clearance oil film; dynamic pressure effect

1. Introduction

The stepped hydrostatic thrust bearing belongs to the full liquid friction bearing, mainly in the hydrostatic mode, and the dynamic pressure plays an auxiliary role. Its high rigidity and high stability require that the working clearance of the bearing is very small. In the very small clearance, the bearing lubricating medium is subject to the combined action of strong shear and strong extrusion, and the heat of the oil film increases, and the oil film becomes thinner and unevenly distributed. At this time, the bearing capacity and accuracy decrease. In severe cases, boundary lubrication or dry friction occurs locally in the bearing friction pair, and then tribological failure occurs. Therefore, scholars have researched hydrostatic

* **Corresponding author: Xiaodong YU**

the main research direction is lubrication theory and bearing development (E-mail：yuxiaodong@hrbust.edu.cn).

thrust bearing from various aspects.

Shaw D has designed a porous oil pad that can be embedded in the groove of the hydrostatic thrust bearing, which improves the hydrodynamic pressure effect and has a higher bearing capacity and stiffness [1]. Singh UP used the Rabinowitsch fluid model to discuss the influence of surface roughness and lubrication inertia of supply area on oil film pressure and bearing capacity of hydrostatic stepped thrust bearing [2,3]. Bouyer J studied the effects of hydrostatic lubrication, mixed lubrication, and hydrodynamic lubrication on the lubrication performance of thrust bearings [4]. Shyu SH studied the effects of plane slider bearings, Rayleigh step bearings, and micro grooved parallel slider bearings on oil film lubrication performance [5]. The combined bearing composed of the water-lubricated hydrostatic thrust bearing and two kinds of radial rolling bearings developed by Lin Shengye has the technical advantages of large axial bearing capacity, small friction power loss, and low-temperature rise [6]. Kodnyanko V has carried out mathematical modeling and theoretical research on the steady and unsteady working modes of adaptive thrust bearing [7]. Venerus DC analyzed the squeeze flow in the lubricating oil film between the porous disk and the impermeable disk of the bearing caused by the relative motion of the disk, and found the analytical solution of the coupling equations controlling the flow in the lubricating oil film and the porous disk [8]. Chien SY proposed the detailed derivation of the Reynolds equation and its corresponding energy equation for the three-dimensional, stable, laminar and compressible flow of single-phase Navi-Stokes fluid in thrust bearings [9]. Tomar AK numerically analyzed the synergistic effect of groove geometry and lubricant nonlinear behavior on 4-cavity spherical radial bearing [10]. Dong investigated the internal flow characteristics of a lobe hydrogen pump for FCV under different rotational speeds by experiments and computational fluid dynamics (CFD). The effects of different rotating speeds on transient pressure pulsation, exhaust flow rate, external noise, and vibration were studied using the dynamic grid calculation method [11]. Sahu K and Sharma SC studied the effects of magnetorheological lubricants and micro groove geometries (rectangular, circular, and triangular) on the lubrication performance of radial bearings [12,13]. Taking the hydrostatic thrust bearing as the research object, Liu YM and Johnson RE discussed the influence of different radial groove lengths, widths, and depths on its bearing capacity [14,15]. Ran HF used the Roelands equation to consider the changes in viscosity, temperature, turbulence, and cavitation and researched the cavitation area of hydrostatic thrust bearing with spiral angle, slot width ratio, rotational speed, and other parameters [16]. Shang YY studied the influence of surface texture shape and height on the bearing performance of hydrostatic thrust bearing and established the change rule of bearing performance under the change of oil supply pressure according to the viscosity-temperature characteristics of lubricating oil [17,18]. Novotný P combines lubrication and heat transfer models to optimize the structure of circular thrust bearings based on genetic algorithms, reducing friction losses by about 30% [19]. Alibeyki. D estimates the heat flux density of the inner surface of the sliding bearing and predicts the bearing temperature. The experiment shows that the accuracy of the heat flux density estimation has a certain regional relationship with the number and location of sensors and the measurement frequency [20]. Baginski P studied the relationship between journal temperature distribution and journal operating parameters and proposed a method to predict bearing temperature distribution [21]. Yan proposes a new load-carrying capacity prediction model for

high-speed orifice plate external pressure hydrogen journal bearings, the results of which agree with those obtained from the finite difference method (FDM) technique [22]. Huang HC designed three kinds of groove layouts of hydrostatic bearings and used ANSYS software to simulate the thermal deformation and structural deformation of the workbench under eccentric load [23]. For the hydrogen circulating pump, Dong studied the leakage clearance distribution of different temperatures and rotor materials, and explored the influencing factors leading to thermal deformation [24]. Yu XD established a three-dimensional simulation model of oil film and friction pair of hydrostatic thrust bearing under high-speed and heavy-load conditions and analyzed the oil film pressure field, temperature field, deformation field of bearing friction pair, and oil film thickness field. The results show that the load causes the turntable and base to undergo inward elastic deformation, and the temperature causes the turntable and base to undergo outward thermal deformation [25-28].

At present, scholars at home and abroad mainly study the oil film pressure, temperature, bearing capacity, stiffness, damping, and eccentricity of hydrostatic thrust bearing with different operating conditions, structural parameters, and viscosity-temperature parameters. These researches play a great role in promoting the development of hydrostatic thrust bearing technology. However, the dynamic pressure effect of the oil film of the stepped hydrostatic thrust bearing is not clear so far. Therefore, according to the hydrodynamics theory, this paper theoretically deduces and calculates the average value of the dynamic pressure of the lubricating oil film in the different clearance height regions for the double rectangular cavity oil cushion, and studies the dynamic pressure effect of the clearance oil film of the multi-oil cushion hydrostatic thrust bearing through the combination of theoretical calculation, simulation, and experimental verification. It provides a theoretical basis for the research on the dynamic pressure performance of hydrostatic thrust bearing in practical engineering.

2 Dynamic pressure lubrication mechanism

2.1 Working principle

The stepped hydrostatic thrust bearing is mainly composed of three parts: rotary worktable, clearance oil film, and base. The base is evenly arranged with twelve oil cushions in the circumferential direction. During operation, the lubricating oil in the oil tank enters the oil cavity of the oil cushion through the oil pump and the oil delivery pipeline in a quantitative way. With the continuous increase of lubricating oil, the gradually rising pressure in the oil cavity will jack up the rotary worktable and load. Under the effect of hydraulic resistance, a layer of oil film with pressure is formed between the oil cavity and the lower surface of the rotary worktable, forming complete liquid friction, and carrying out high stability work. The geometric model of hydrostatic thrust bearing is shown in Fig. 1, and the structural parameters are shown in Table 1.

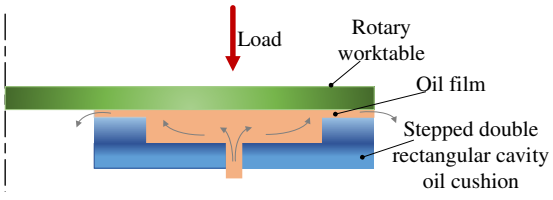

Fig.1 Geometric model of hydrostatic thrust bearing

Table 1 Structural parameters

Parameter	Value	Parameter	Value

Worktable diameter	3.15m	Outer diameter of guide rail r_2	975mm
Weight of worktable	9.85t	Inner diameter of guide rail r_1	692.5mm
Oil film thickness h_0	0.1mm	Number of oil cushions	12
Bearing range	0~32t	Speed range	1~250r/min
Diameter of the oil inlet	15mm	Total length of oil cavity L	300mm
Oil cavity depth	3mm	Total width of oil chamber B	190mm
Width of Sealing edge	11mm	Width of oil return groove	10mm

2.2 Bearing characteristics of dynamic pressure

The structure of the oil cushion with double rectangular cavities is shown in Fig. 2. The Reynolds number is used to judge the movement state of the fluid in the oil cushion. The calculation shows that the maximum flow rate of lubricating oil at the inlet is not more than 0.32m/s, the Reynolds number at the inlet of the oil cushion is 69.588, the Reynolds number is 1373.308 by introducing hydraulic radius into the oil cavity, and the Reynolds number at the outlet of sealing edge of oil cushion is 46.828 by introducing the hydraulic radius. Therefore, the Reynolds number of the three parts is less than 2320, so it is assumed that the whole oil film flow state is laminar flow, and with the increase of rotational speed, there is no possibility of laminar flow to turbulent flow within the range of rotational speed in this study.

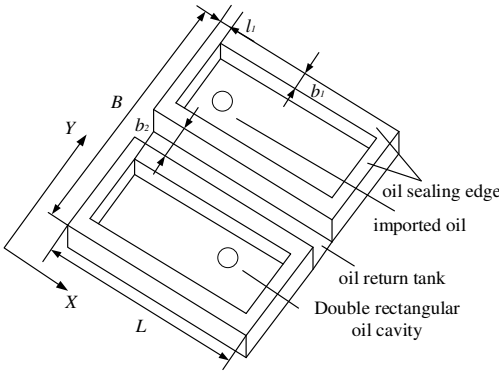

Fig. 2 Structure of double rectangular cavity oil cushion

As shown in Fig. 3, coordinate systems are established in areas L_1 and L_2 respectively. The height of the lubricating oil film of the stepped hydrostatic thrust bearing is in region L_1, $h=h_1$, and in region L_2, $h=h_2$.

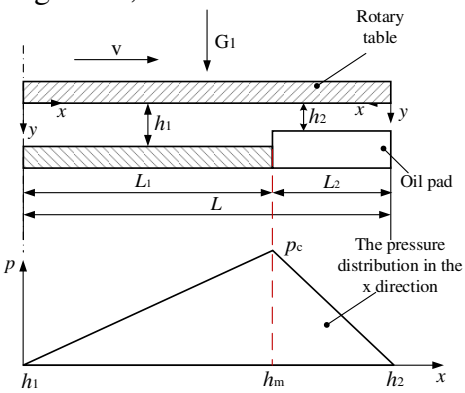

Fig. 3 Pressure distribution of oil film with equal clearance

The expression of the dynamic pressure effect of stepped hydrostatic thrust bearing is:

In region L_1, the basic equation of dynamic pressure bearing is:

$$\frac{dp}{dx}=6\mu v\frac{h-h_m}{h^3} \tag{1}$$

In region L_2, the basic equation of dynamic pressure bearing is:

$$\frac{dp}{dx}=6\mu v\frac{h_m-h}{h^3} \tag{2}$$

For region L_1, $C_1=0$ is determined according to boundary conditions

$$\begin{cases} x=0, p=0 \\ x=L_1, P=P_C \end{cases},$$

$$P_{C1}=6\mu v\frac{h_1-h_m}{h_1^{\,3}}L_1 \tag{3}$$

Similarly, for region L_2, there is $C_1=0$,

$$P_{C2}=6\mu v\frac{h_m-h_2}{h_2^{\,3}}L_2 \tag{4}$$

Since Pc is the public pressure at the ladder, there is $P_{C1}=P_{C2}$, namely:

$$6\mu v\frac{h_1-h_m}{h_1^{\,3}}L_1=6\mu v\frac{h_m-h_2}{h_2^{\,3}}L_2 \tag{5}$$

There are:

$$h_m=\frac{h_1h_2\left(L_1h_2^{\,2}+L_2h_1^{\,2}\right)}{L_1h_2^{\,3}+L_2h_1^{\,3}} \tag{6}$$

The pressure distribution of the two regions is obtained as follows:

$$\begin{cases} P_{L1}(x)=\dfrac{6\mu v}{h_1^{\,2}}\left[1-\dfrac{h_2\left(L_1h_2^{\,2}+L_2h_1^{\,2}\right)}{L_1h_2^{\,3}+L_2h_1^{\,3}}\right]x \\ P_{L2}(x)=\dfrac{6\mu v}{h_2^{\,2}}\left[\dfrac{h_1\left(L_1h_2^{\,2}+L_2h_1^{\,2}\right)}{L_1h_2^{\,3}+L_2h_1^{\,3}}-1\right]x \end{cases} \tag{7}$$

The average pressure of the two regions is $P=P_{L1}+P_{L2}$.

Then the dynamic pressure bearing capacity is:

$$W=B\left(\int_0^{L_1}P_{L1}(x)dx+\int_0^{L_2}P_{L2}(x)dx\right) \tag{8}$$

Substitute $P_{L1}(x)$ and $P_{L2}(x)$ obtain:

$$W=\frac{3\mu vBL_1L_2Lt}{L_1h_2^{\,3}+L_2h_1^{\,3}} \tag{9}$$

Where, $L_1=L/2-l_1$, $L_2=l_1$, $h_1=h+t$, $h_2=h$, $v=r\omega$

Through analysis, it can be found that the dynamic pressure bearing of the lubricating oil film of the stepped hydrostatic thrust bearing mainly depends on the structural size of the oil cushion, the viscosity of the lubricating oil, and the rotating speed of the workbench, and has nothing to do with the load. When the structural dimension parameters, initial oil film thickness, and lubricating oil viscosity of the oil cushion are fixed, the rotating speed of the workbench becomes the main factor of the dynamic pressure bearing of the hydrostatic thrust bearing. The higher the rotating speed is, the greater the dynamic pressure bearing is, and with the increase in the rotating speed, the dynamic pressure value shows a linear growth trend.

2.3 Theoretical study on dynamic pressure effect of clearance oil film

According to the different rotating speeds of the workbench, the dynamic viscosity of 46-HL lubricating oil at 30℃ is used to calculate the dynamic pressure of the clearance oil film of the stepped hydrostatic thrust bearing. The calculation results are shown in Fig. 4.

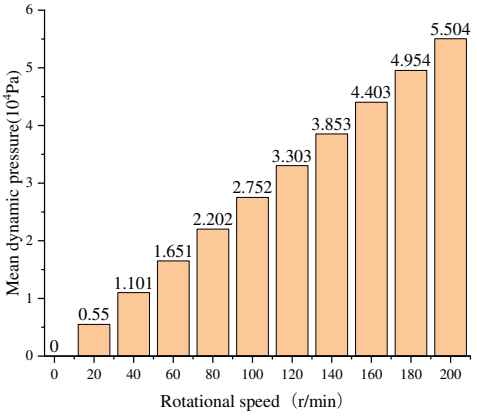

Fig. 4 Theoretical calculation of dynamic pressure at different rotational speeds

It can be seen from Fig. 4 that the dynamic pressure of the hydrostatic thrust bearing increases linearly with the increase of the rotating speed of the workbench. When the rotating speed of the workbench is 0r/min, there is no dynamic pressure in theory.

3 Finite Element Model and Boundary Conditions of Clearance Oil Film

3.1 Model of clearance oil film

The three-dimensional model is established by SolidWorks. The clearance oil film model and boundary condition setting of the double rectangular cavity oil cushion are shown in Fig. 5(a). The oil film model is imported into ICEM-CFD, and the structured regular hexahedron mesh is used to define the part, slice, topological structure, association mapping, and O-grid division of the oil inlet hole. The final result is that the total number of grids is 869864, the overall quality of the grid is greater than 0.728, and the minimum angle is 45 °, which is far higher than the grid evaluation criteria, meeting the subsequent simulation requirements.

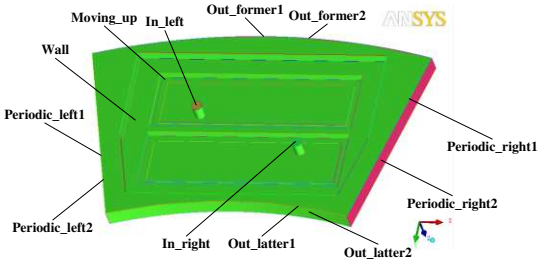

(a)

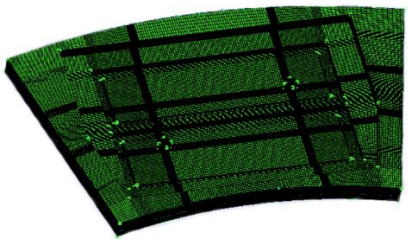

(b)

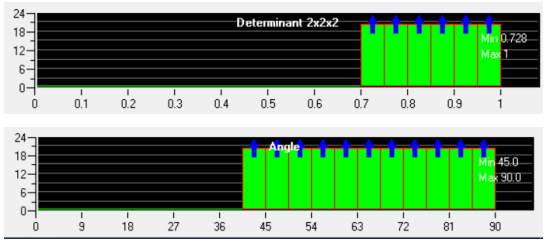

(c)

Fig. 5 Oil film model. (a) Oil film model and boundary condition setting; (b) Model of oil film grid; (c) Quality of oil film mesh

In order to better obtain the simulation results of the dynamic pressure effect, the mathematical model and lubricating oil film simulation are subject to conditional assumptions: the selected 46-HL lubricating oil is an incompressible fluid, and the formed wedge-shaped oil film fluid is a three-dimensional steady flow, ignoring the influence of the centrifugal force of the rotary worktable, and the fluid and the wall of the rotary worktable are free of slip.

3.2 Viscosity-temperature relationship

According to the actual working conditions of the stepped hydrostatic thrust bearing, 46-HL lubricating oil is selected for simulation. Table 2 shows the physical parameters of 46-HL lubricating oil.

Table 2 Viscosity-temperature parameters of 46-HL lubricating oil

Celsius temperature (℃)	20	30	40	50	60	70
Dynamic viscosity($10^{-2}Pa\cdot s$)	11.1408	6.069312	3.6432	2.3391	1.312	1.13256

Since the maximum temperature of the studied clearance oil film is not more than 60℃, the dynamic viscosity of lubricating oil at 20℃, 40℃ and 60℃ are selected to be substituted into Vogel's viscosity-temperature equation, and the viscosity-temperature equation expression is obtained by solving three sets of linear equations:

$$\mu = Ae^{\frac{B}{T+C}}$$

$$\mu = 1.90592291561894 \times 10^{-10} e^{\frac{10501.5756386481}{T+130.445836936273}} \quad (10)$$

Where, μ is the dynamic viscosity (10^{-2}Pa •s), and T is the average temperature (K).

3.3 Initial value verification

During the numerical simulation, the accuracy of the initial value is of great significance to the whole research results. Therefore, based on the initial value of static pressure when the hydrostatic worktable is jacked up, the initial static pressure of oil film under different loads is verified at the speed of 0r/min. The initial pressure field of oil film with a load of 5t and 15t is listed here, as shown in Fig. 6. The pressure comparison between theoretical calculation value and numerical simulation value under different loads is shown in Table 3.

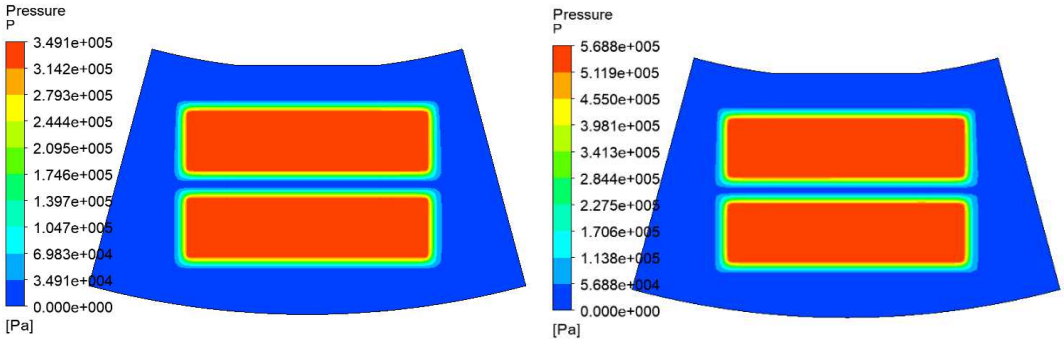

(a) (b)

Fig. 6 Initial pressure field of oil film. (a) Load 5t; (b) Load 15t

Table 3 Verification of initial pressure value of theoretical calculation and numerical simulation under different loads

Average pressure	Load（t）						
（×10^5Pa）	0	5	10	15	20	25	30
Theoretical calculation	1.7617	2.6559	3.5502	4.4444	5.3387	6.2329	7.1272
Numerical simulation	1.8267	2.8286	3.7436	4.6164	5.7870	6.9679	8.1226
Error rate	3.56%	6.11%	5.17%	3.73%	7.75%	10.54%	12.25%

According to the table data analysis, there is a certain error between the average pressure of numerical simulation and theoretical calculation, but the maximum error rate is less than 13%, which is within the controllable error range. Therefore, the simulated pressure value is basically consistent with the theoretical pressure value, and the oil cavity pressure is proportional to the load. The numerical simulation pressure conforms to the theoretical expectation, so the initial value of the simulation can be considered the correct value. Because the initial pressure error is not large, the oil film dynamic pressure effect of stepped hydrostatic thrust bearing under different working conditions can be simulated and analyzed on this basis.

4 Simulation study on dynamic pressure effect of clearance oil film

4.1 Numerical simulation

FLUENT is used to simulate the oil film model of the double rectangular cavity oil cushion of the stepped hydrostatic thrust

bearing under the condition of variable viscosity, and the workbench rotates counterclockwise to finally obtain the oil film dynamic pressure field program. Due to space limitation, only the program of pressure field with a load of 10t and 20t and rotating speed of 60r/min, 100r/min, and 140r/min are listed here, as shown in Fig. 7.

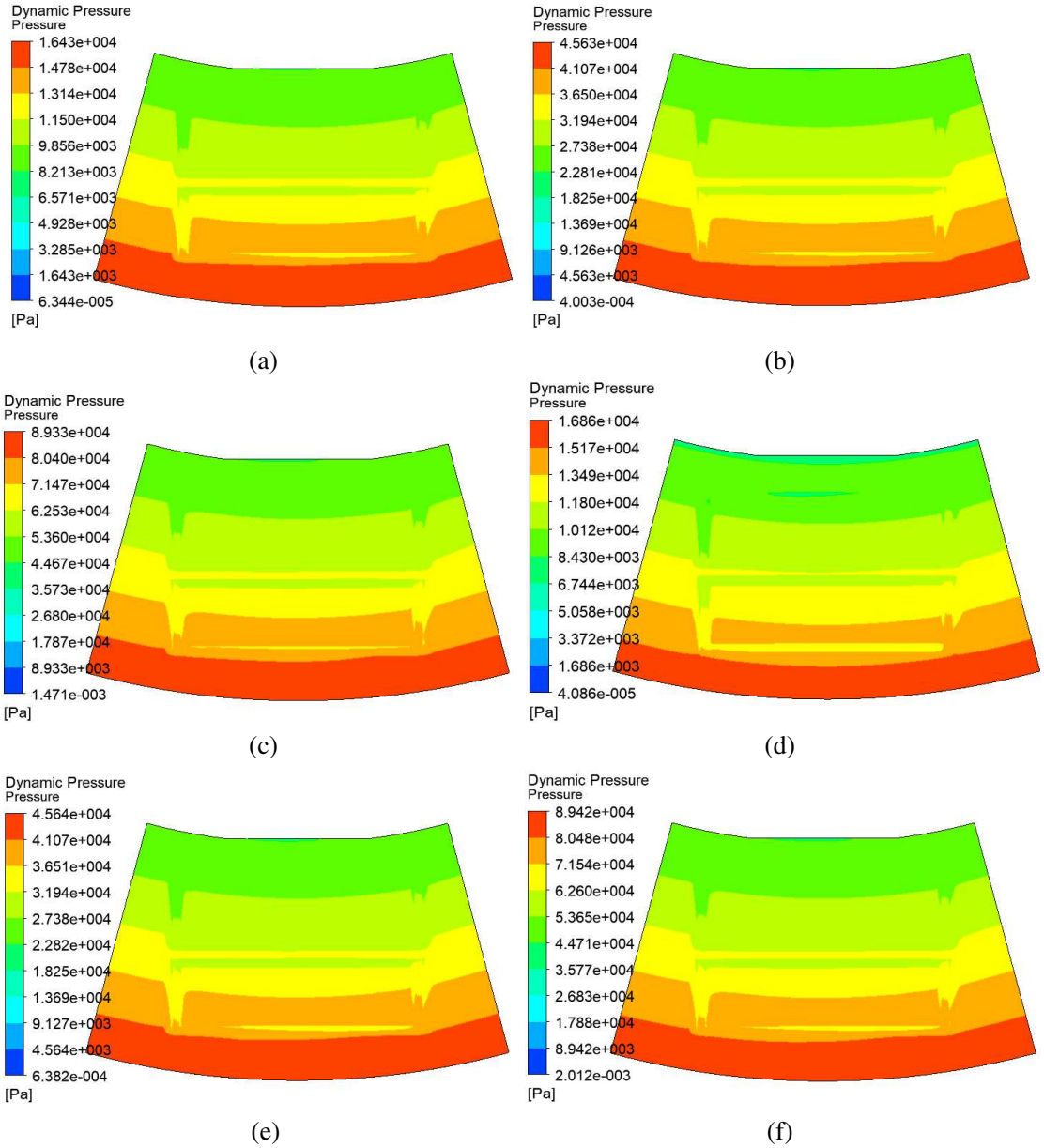

Fig. 7 Simulation program of the partial dynamic pressure field. (a) 10t-60r/min; (b) 10t-100r/min; (c) 10t-140r/min; (d) 20t-60r/min; (e) 20t-100r/min; (f) 20t-140r/min

According to the partial dynamic pressure field simulation program in Fig. 7, it is obvious that the radial dynamic pressure value of a single oil film increases in a stepped fashion from the inside to the outside. This is because the linear velocity on the outside of the oil cushion is greater than the linear velocity on the inside of the oil cushion. The larger the linear velocity is, the greater the corresponding dynamic pressure value is. It can also be found that when the rotating speed increases from 60r/min to 140r/min and the load is 10t, the maximum dynamic pressure value changes from 1.6426×104Pa increases to 8.9333×104Pa, the

average dynamic pressure value is from 0.6515×10^4Pa increases to 3.3887×10^4Pa ; When the load is 20t, the maximum dynamic pressure value is from 1.6861×10^4Pa increases to 8.9423×10^4Pa, the average dynamic pressure value is from 0.6506×10^4Pa increases to 3.4207×10^4Pa. It can be seen that the value of dynamic pressure is related to the rotating speed of the workbench, and the greater the rotating speed, the greater the dynamic pressure value, which is consistent with the theoretical results.

To show the distribution of dynamic pressure in the whole oil cushion, the oil film model with double rectangular cavities is divided into line segments in the absolute rectangular coordinate system, as shown in Fig. 8. In the whole oil film model, the coordinates of the radial left side (line-jx-zc) are (-86, -692.5), (-160,-975), and the coordinates of the radial right side (line-jx-yc) are (86, -692.5), (16,-975); The coordinates of the circumferential inner side (line-zx-nc) are (245, -775), (-245, -775), and the circumferential outer side (line-zx-wc) are (260, -875), (-260, -875). The unit is mm. They intersect with the Z=0 plane (the boundary layer in contact with the rotary worktable) respectively, and the intersection lines along the radial and circumferential distribution are obtained. The pressure values of each point on the intersection line are analyzed by the post-processing module of FLUENT, as shown in Fig. 9.

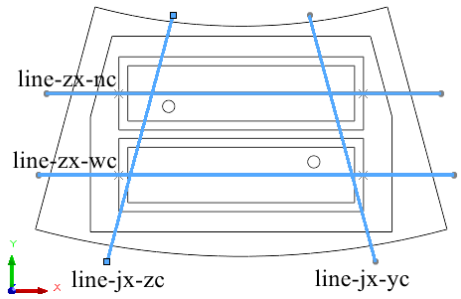

Fig. 8 Division of plane position

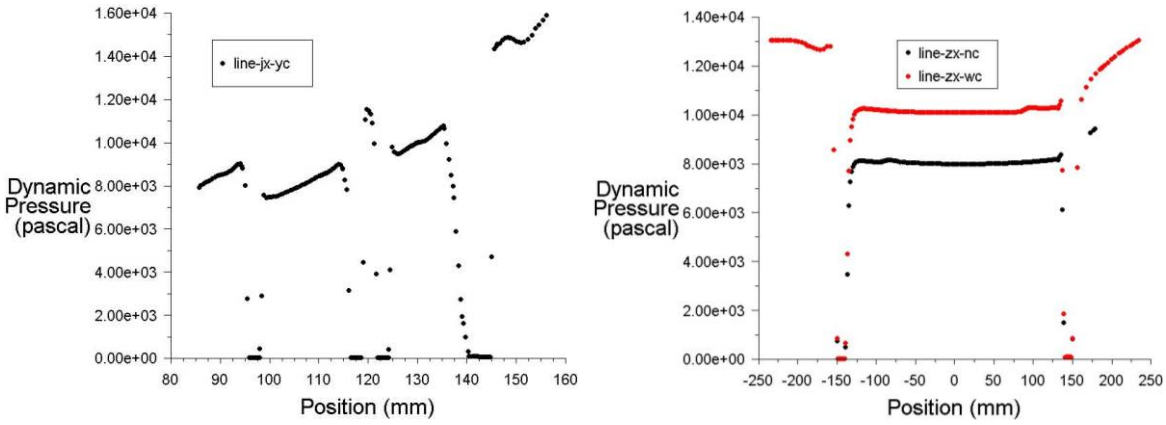

(a)

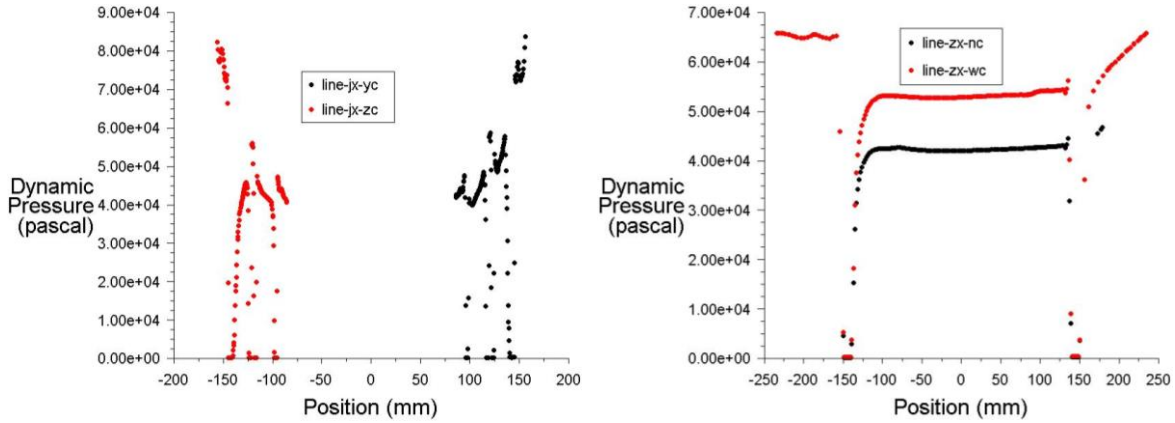

(b)

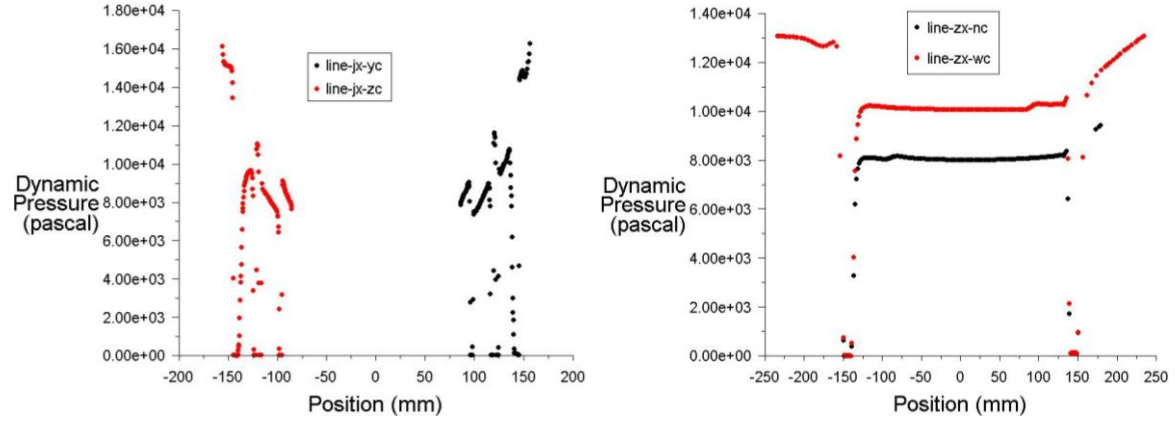

(c)

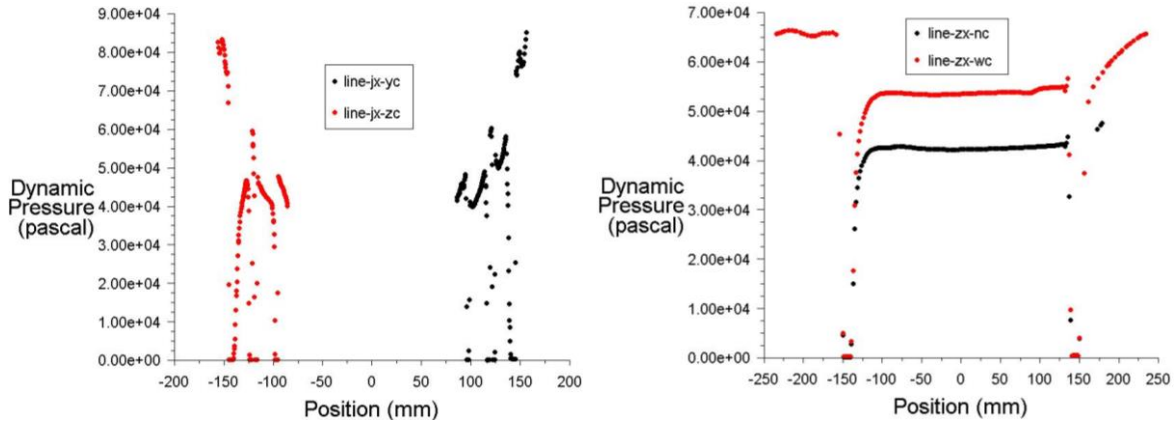

(d)

Fig. 9 Scatter diagram of pressure distribution under some working conditions. (a) 10t-60r/min; (b) 10t-140r/min; (c) 20t-60r/min; (d) 20t-140r/min

According to the line-jx-yc diagram in Fig. 9(a), the dynamic pressure at the sealing oil edge around the oil cavity is linearly distributed, and the value is basically 0; The dynamic pressure value gradually increases along the radial direction of the oil cushion, and the maximum value appears at the outermost side of the double rectangular cavity oil cushion. According to the abscissa of line-zx-nc and line-zx-wc scatter plots, the rectangular oil cavity part of the double rectangular oil cushion is located in the range of -139mm to 139mm. The dynamic pressure value of the oil film under different working conditions is similar to

a horizontal line, and the average dynamic pressure value of the outer rectangle is greater than that of the inner rectangle, indicating that the dynamic pressure value of the oil film inside the rectangular oil cavity is relatively stable, the outer rectangle is far from the center of rotation, the linear velocity is high, and the dynamic pressure value is relatively large. The position range from -150mm to -139mm and 139mm to 150mm is part of the oil sealing edge on the left and right sides of the rectangular cavity oil cushion in the circumferential direction. It is found that the dynamic pressure value has an upward trend at the junction of the right oil cavity and the oil sealing edge in the circumferential direction, and then drops to 0 after reaching the peak value. This is because the oil film meets the dynamic pressure formation conditions when flowing into the oil sealing edge from the oil cavity, and strong dynamic pressure is generated here. When the oil film passes through the oil sealing edge, the distance between the oil sealing edge and the bottom surface of the rotary worktable is fixed, and the conditions for forming dynamic pressure are lost. Therefore, the dynamic pressure gradually decreases to 0. The position range from -245mm to -150mm and 150 mm to 245mm is the oil return groove part of the rectangular cavity oil cushion. The dynamic pressure value of the circumferential right oil return groove part gradually increases, and the dynamic pressure value of the left oil return groove part gradually decreases. This is because the dynamic pressure phenomenon also occurs when the oil film flows into the oil return groove from the sealing edge, resulting in the pressure value gradually increasing. The 12 double rectangular cavity oil cushions are uniformly distributed on the base of the workbench, and the workbench rotates counterclockwise, as a result, when the lubricating oil flows into the oil return groove on the left side of the adjacent oil cushion and the condition for forming dynamic pressure is lost, the dynamic pressure value gradually decreases until the left oil sealing edge decreases to 0, and then circulates in turn.

4.2 Comparative analysis

The simulation results of the average dynamic pressure value at the load of 0t, 5t, 10t, 15t, 20t, 25, and 30t and the rotating speed of 0r/min-200r/min are sorted out and compared with the theoretically calculated dynamic pressure value at different rotating speeds. The comparison curve is shown in Fig. 10. Then, the curve fitting of the average dynamic pressure value of theoretical calculation and simulation is carried out, as shown in Fig. 11 and Fig. 12. The curve fitting data of the simulation is the average value of the average dynamic pressure value under different loads.

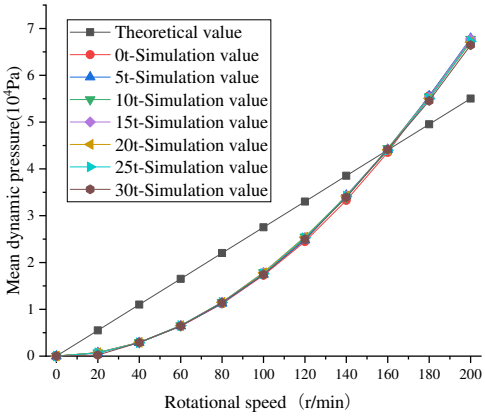

Fig. 10 Comparison curve of theoretical and simulated dynamic pressure values

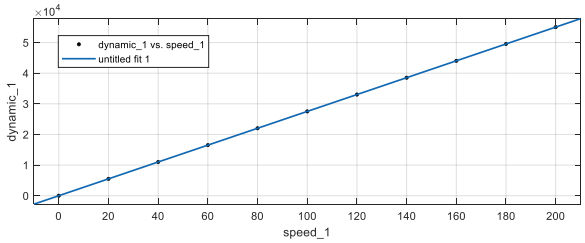

Fig. 11 Curve fitting of theoretical calculation

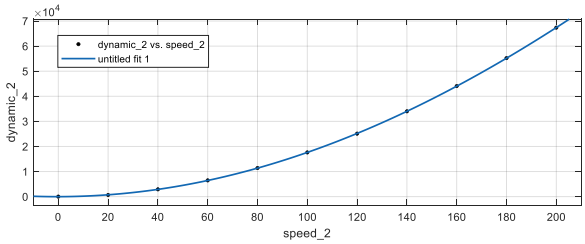

Fig. 12 Curve fitting of simulation

It can be seen from Fig. 10 that under constant load, the simulated value of the average dynamic pressure of the oil film increases with the increase of the speed. At constant speed, the simulated value of the average dynamic pressure of the oil film fluctuates slightly with the increase of the load, which is consistent. This shows that the increase in the average dynamic pressure is independent of the load, which is consistent with the previous theoretical results. When the rotating speed is lower than 160r/min, the simulated value of the average dynamic pressure of the oil film shows a concave growth and is lower than the theoretical calculation value. At this time, the shear heat of the oil film is small, the rise of oil film temperature is small, the exponential function of lubricating oil viscosity has a small variation range, and the numerical value is large, but the rotational speed is low, resulting in low simulation value. When the rotating speed is higher than 160r/min, the oil film shear heat is serious, the oil film temperature continues to rise, and the viscosity of lubricating oil changes greatly, which is small in value, but the rotating speed is high, resulting in a higher simulation value. It can be seen that in the speed range of 0r/min-200r/min, compared with the viscosity of lubricating oil, the speed is the main factor affecting the dynamic pressure value of the oil film of the stepped hydrostatic thrust bearing.

From the fitting curve in Fig. 11, it can be concluded that the fitting function is $y = 275.2x - 0.09091$ (x represents rotational speed, in r/min, y represents dynamic pressure value, in Pa), which shows that the theoretical value of average dynamic pressure increases with the increase of rotational speed in a linear relationship with a slope of 275.2.

According to the fitting curve in Fig. 12, the fitting function is

$$y = 223400\text{-}223500 \times \cos(0.003977x) + 517.2 \times \sin(0.003977x)$$

(the unit is the same as above), which is called the Fourier1 model. That is, the simulation value of average dynamic pressure does not increase linearly with the increase of rotating speed, because the viscosity of lubricating oil is fixed in the theoretical calculation, and the dynamic pressure value is linear with rotating speed. To make the results more accurate, the variable viscosity is used in the simulation. The viscosity-temperature equation of the variable viscosity is an exponential function. Therefore, the simulated value of average dynamic pressure increases with the increase of rotating speed in the way of the Fourier 1 model.

5 Experimental study on dynamic pressure effect of the clearance oil film of double rectangular cavities

5.1 Experimental equipment and scheme

The experiment was carried out on the high-speed and heavy-load hydrostatic thrust bearing testbench with model Q1-224. Its actual size is consistent with that of the three-dimensional model in the text, as shown

in Fig. 13. Twelve double rectangular oil cushions are uniformly distributed on the hydrostatic bearing base. According to the simulation, the pressure field in the inner and outer cavities of the oil cushion with double rectangular cavities is uneven. Therefore, six pressure sensors are selected to be installed in the inner and outer oil cavities respectively.

(a) (b)

Fig. 13 Hydrostatic thrust bearing testbench. (a) The testbench; (b) Installation position of the pressure sensor

Select the load of 10t and 20t, the hydraulic oil model is HL-46, and the test step is 20r/min, from 20r/min to 200r/min, to carry out the experimental study on the dynamic pressure effect of the clearance oil film. In order to improve the accuracy of the experimental results, the average value of four repeated measurements was taken at each monitoring point.

5.2 Experimental results and analysis

Due to space limitation, only the dynamic pressure test data values of each monitoring point corresponding to different rotating speeds at 10t load are listed here, as shown in Table 4.

Table 4 Oil film dynamic pressure test results from 20r/min to 200r/min under 10t load (unit: 10^4Pa)

Sensor number	P1	P2	P3	P4	P5	P6
20r/min	0.732	0.706	0.673	0.181	0.202	0.235
40r/min	1.194	1.137	1.082	0.583	0.506	0.584
60r/min	1.638	1.6	1.564	0.661	0.746	0.795
80r/min	2.185	2.143	2.036	1.053	1.126	1.165
100r/min	2.703	2.652	2.614	1.815	1.853	1.895
120r/min	3.278	3.244	3.207	2.194	2.237	2.268
140r/min	3.974	3.952	3.917	2.893	2.924	2.957
160r/min	5.294	5.255	5.206	3.598	3.612	3.677
180r/min	5.684	5.626	5.583	4.486	4.51	4.547
200r/min	6.246	6.215	6.182	5.084	5.073	5.117

The dynamic pressure test data of each monitoring point are sorted out, and the relationship curve of the dynamic pressure of the oil cavity with the change of speed is obtained for the load of 10t and 20t, as shown in Fig. 14 and Fig. 15.

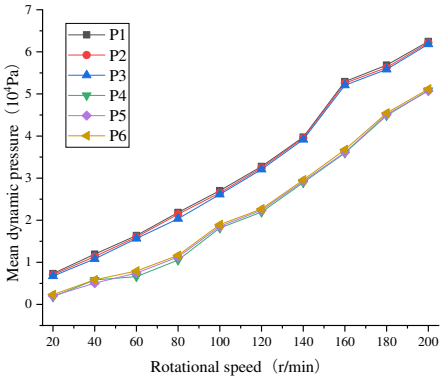

Fig. 14 Dynamic pressure value at each monitoring point with a load of 10t

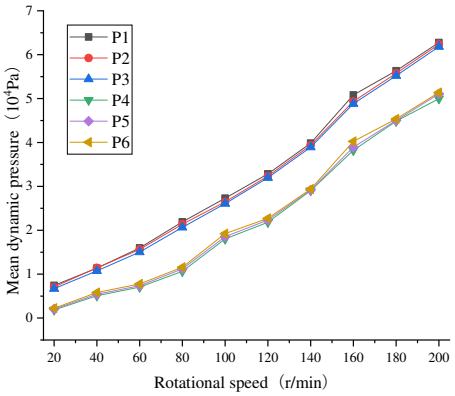

Fig. 15 Dynamic pressure value at each monitoring point with a load of 20t

From the dynamic pressure values of each monitoring point in Fig. 14 and Fig. 15, it can be found that the overall dynamic pressure distribution of the double rectangular cavity is inconsistent, but both increase with the increase of the rotating speed. The overall fluctuation range of the dynamic pressure value under the load of 10t and 20t is the same, which verifies the results of theoretical calculation and simulation, that is, the increase of the average dynamic pressure value is independent of the load. It can also be found that the oil film dynamic pressure values of monitoring points P1, P2, and P3 in the outer rectangle of the double rectangular oil cushion are higher than those of monitoring points P4, P5, and P6 in the inner rectangle, which is consistent with the simulation results, that is, the outer rectangle is far from the center of rotation, and the linear velocity is higher, so the dynamic pressure value is higher.

The comparison curves of the theoretical, simulation, and experimental changes of the average dynamic pressure with the rotational speed under the load of 10t and 20t are given below, as shown in Fig. 16. The experimental value is the average dynamic pressure of six sensors.

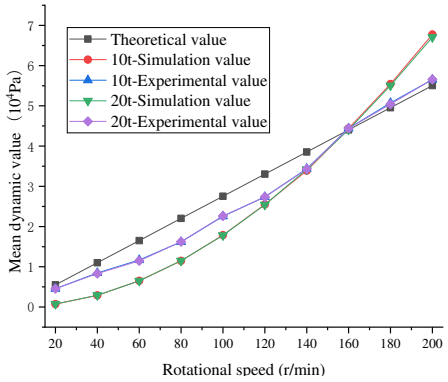

Fig. 16 Dynamic pressure curve of theory-simulation-experiment

It can be seen from Fig. 16 that the experimental value of the average dynamic pressure of different loads at the same speed is basically the same. With the increase in rotating speed, the experimental value of the average dynamic pressure is between the theoretical calculation value and the simulation value. This is because the pressure sensor monitors the average dynamic pressure value of the micro plane in the form of a small hole. In the simulation process, the probe monitors the average dynamic pressure value of each point, while in the theoretical calculation, the average dynamic pressure value of the whole oil cavity surface is taken. There is a certain deviation between the position of the point, the micro plane, and the whole plane.

The consistency between the variation law of the average dynamic pressure value with the speed and load monitored by the experiment and the results of theoretical calculation and simulation shows that the theoretical calculation and simulation results of the clearance oil film of the stepped hydrostatic thrust bearing are correct, which further proves the correctness of the dynamic pressure effect model.

6 Conclusion

In this paper, the dynamic pressure effect of the clearance oil film of a stepped hydrostatic thrust bearing with a double rectangular cavity oil cushion is studied. The average value of the dynamic pressure of the lubricating oil film in different height regions is theoretically derived and calculated. The dynamic pressure effect of the clearance oil film of the hydrostatic thrust bearing is obtained for the first time through the simulation of the dynamic pressure field, the dynamic pressure distribution scatters diagram, and the dynamic pressure value of each monitoring point in the experiment. The correctness of the dynamic pressure effect model is verified through the comparison of theoretical calculation, simulation, and experimental data. It provides a theoretical basis and idea for the study of the hybrid lubrication performance of hydrostatic thrust bearings and provides a research direction for the machining accuracy and operation stability of high-speed and heavy-duty CNC equipment.

(1) The overall dynamic pressure effect of the clearance oil film of stepped hydrostatic thrust bearing is as follows: the average dynamic pressure increases with the increase of the rotating speed of the workbench, which is basically independent of the load. Among them, the theoretical value of the average dynamic pressure and the rotational speed show a linear growth relationship with a slope of 275.2. The simulated value of the average dynamic pressure and the rotational speed follow the growth law of the Fourier 1 model. In the speed range of 0r/min-200r/min, compared with the viscosity of lubricating oil, the speed is the main factor affecting the dynamic pressure value of the oil film of the stepped hydrostatic thrust bearing.

(2) The specific analysis of the dynamic pressure effect of the clearance oil film shows that the dynamic pressure value gradually increases along the radial direction of the oil cushion, and the maximum value appears at the outermost side of the double rectangular cavity oil cushion. The dynamic pressure value at the oil sealing edge of the oil cushion is basically 0, and the dynamic pressure value of the oil film inside the double rectangular oil cavity is relatively stable. At the junction of the circumferential right oil cavity and the oil sealing edge, it is found that the dynamic pressure value has an obvious upward trend, and then decreases to 0 after reaching the peak value.

(3) The dynamic pressure oil film monitoring is carried out on the high-speed and heavy-duty hydrostatic thrust bearing test bench with model Q1-224. The Experimental value of average dynamic pressure between the theoretical calculation value and the simulation value as the speed increases. The dynamic pressure of the oil film of the outer rectangle of the double rectangular cushion is higher than that of the inner rectangle, which is consistent with the simulation results.

Declaration of competing interest

The authors declare that they have no known competing financial interests or personal relationships that could have appeared to influence the work reported in this paper.

Acknowledgement

The author(s) disclosed receipt of the following financial support for the research, authorship, and/or publication of this article. This financial support for this work was provided by National Key Research and Development Project (2022YFB3404902).

Reference

[1] Shaw, D., Hsieh, H.A.: Hydrostatic journal bearing with porous pads and improved properties. J. Tribol.-Trans. ASME. **141**(12),1-36 (2019)

[2] Singh, U.P., Sinha, P., Kumar, M.: Analysis of hydrostatic rough thrust bearing lubricated with Rabinowitsch fluid considering fluid inertia in supply region. Proc. Inst. Mech. Eng. Part J.-J. Eng. Tribol. **235**(2), 386-395 (2021)

[3] Singh, U.P., Gupta, R.S., Kapur, V.K.: On the application of Rabinowitsch fluid model on an annular ring hydrostatic thrust bearing. Tribol. Int. **58**, 65-70 (2013)

[4] Bouyer, J., Wodtke, M., Fillon, M.: Experimental research on a hydrodynamic thrust bearing with hydrostatic lift pockets: Influence of lubrication modes on bearing performance. Tribol. Int. **165**, (2021)

[5] Shyu, S.H., Hsu, W.C.: A numerical study on the negligibility of cross-film pressure variation in infinitely wide plane slider bearing, Rayleigh step bearing and micro-grooved parallel slider bearing. Int. J. Mech. Sci. **137**, 315-323 (2018)

[6] Lin, S.Y., Jiang, S.Y.: Rotordynamics of an improved face-grinding spindle: rotational stiffness of thrust bearing increases radial stiffness of spindle. J. Manuf. Sci. Eng.-Trans. ASME. **144**(8), (2022)

[7] Kodnyanko, V., Kurzakov, A., Grigorieva, O.: Theoretical disquisition on the static and dynamic characteristics of an adaptive stepped hydrostatic thrust bearing with a displacement compensator. Mathematics. **9**(22), (2021)

[8] Venerus, D.C.: Squeeze flows in liquid films bound by porous disks. J. Fluid Mech. **855**, 860-881 (2018)

[9] Chien, S.Y., Cramer, M.S.: Compressible high-pressure lubrication flows in thrust bearings. J. Fluid Mech. **939**, (2022)

[10] Tomar, A.K., Sharma, S.C.: Non-Newtonian lubrication of hybrid multi-recess spherical journal bearings with different geometric shapes of recess. Tribol. Int. **171**, (2022)

[11] Dong, L., Zhou, R.Z., Liu, H.L.: Effect of rotational speed on unstable characteristics of lobe hydrogen circulating pump in fuel cell system. Int. J. Hydrog. Energy. **47**(50), 21435-21449 (2022)

[12] Sahu, K., Sharma, S.C., Ram, N.: Misalignment and surface irregularities effect in MR fluid journal bearing. Int. J. Mech. Sci. **221**, (2022)

[13] Sharma, S.C., Tomar, A.K.: Study on MR fluid hybrid hole-entry spherical journal bearing with micro-grooves. Int. J. Mech. Sci. **202**, (2021).

[14] Liu, Y.M., Cao, Z.F., Zhang, Y.: Design and research of symmetrical multi-throttle thrust hydrostatic bearing based on comparative analysis of various meshes. Symmetry-Basel. **14**(2), (2022)

[15] Johnson, R.E., Manring, N.D.: Translating circular thrust bearings. J. Fluid Mech. **530**, 197-212 (2005)

[16] Ran, H.F., Dai, P., Yan, S.P.: Flow mechanisms

and lubrication performance of water-lubricated thrust bearings with herringbone grooves. Lubricants. **10**(8), (2022)

[17] Shang, Y.Y., Cheng, K., Ding, H.: Design and optimization of the surface texture at the hydrostatic bearing and the spindle for high precision machining. Machines. **10**(9), (2022)

[18] Shang, Y.Y., Cheng, K., Ding, H.: Design of a hydrostatic spindle and its simulation analysis with the application to a high precision internal grinding machine. Machines. **10**(2), (2022)

[19] Novotný, P., Jonák, M., Vacula, J.: Evolutionary optimisation of the thrust bearing considering multiple operating conditions in turbomachinery. Int. J. Mech. Sci. **195**, (2021)

[20] Alibeyki, D., Mehryar, R.: Heat flux estimation in journal bearings using inverse heat transfer method. Heat Mass Transf. **57**(4), 605-615 (2021)

[21] Baginski, P., Zywica, G., Roemer, J.: Experimental study of the influence of rotor dynamics on the temperature distribution of a gas foil bearing. Appl. Sci.-Basel. **12**(18), (2022)

[22] Yan, H., Ke, C.L., Peng, N.: Performance prediction of externally pressurized gas bearings for high-speed turbo-expander involving hydrogen, helium and air working fluids. Int. J. Hydrog. Energy. (46-67), 33453-33467 (2021)

[23] Huang, H.C., Yang, S.H.: Thrust-bearing layout design of a large-sized hydrostatic rotary table to withstand eccentric loads for horizontal boring machine applications. Lubricants. **10**(4), (2022)

[24] Dong, K., Liu, G., Yang, Q.: Effect of thermal deformation on leakage clearance of claw hydrogen circulating pump for fuel cell system. Int. J. Hydrog. Energy. **47**(66), 28655-28669 (2022)

[25] Yu, X.D., Wang, Y., Zhou, D.F.: Heat transfer characteristics of high speed and heavy load hydrostatic bearing. Ieee Access **7**, 110770-110780 (2019)

[26] Yu, X.D., Wang, F.K., Zhou, D.F.: Deformation characteristics of adaptive hydrostatic thrust bearing under extreme working conditions. J. Braz. Soc. Mech. Sci. Eng. **42**(9), (2020)

[27] Yu, X.D., Tang, B.Y., Wang, S.B.: High-speed and heavy-load tribological properties of hydrostatic thrust bearing with double rectangular recess. Int. J. Hydrog. Energy. **47**(49), 21273-82126 (2022)

[28] Yu, X.D., Feng, Y.N., Gao, W.C.: Study on lubrication performance of hydrostatic clearance oil film considering multi-factor coupling. Int. J. Hydrog. Energy. **47**(94), 40083-40098 (2022)